Silver-Bismuth Halide Double Salts for Lead-free Photovoltaics: Insights From Symmetry-Based Modeling

Supporting Information

Bruno Cucco[†], Laurent Pedesseau[‡], Claudine Katan[†], Jacky Even[‡], Mikaël Kepenekian[†]*, and George Volonakis[†]*

[†] *Univ Rennes, ENSCR, INSA Rennes, CNRS, ISCR - UMR 6226, Rennes, France*
[‡] *Univ Rennes, INSA Rennes, CNRS, Institut FOTON - UMR 6082, Rennes, France*
**email: mikael.kepenekian@univ-rennes1.fr; george.volonakis@univ-rennes1.fr*

1 Computational methods

All the calculations in this work are performed within the DFT framework using Quantum ESPRESSO Suite.[1,2] All the structures are relaxed with a 80 Ry cutoff for the plane-wave kinetic energy with a converged $8 \times 8 \times 8$ Brillouin zone sampling. The threshold on forces and total energy during ionic minimization were converged to 10^{-6} alongside a threshold of 10^{-10} for the SCF steps. All the calculations are performed using fully-relativistic norm-conserving PBE pseudopotential[3] taken from the pseudo-dojo database (http://www.pseudo-dojo.org). The optical absorption calculations are performed using the YAMBO[4] code. Calculation are performed within random phase approximation (RPA) employing a dense $16 \times 16 \times 16$ k-point grid and 800 bands. Furthermore, the optical spectra is scissor shifted to match the PBE0 band gap. The hybrid DFT-PBE0 calculations are performed using a $4 \times 4 \times 4$ k-grid sampling with a $2 \times 2 \times 2$ q-grid sampling for the Fock operator. The hybrid band structures are interpolated using the code Wannier90.[5] We employed a fine $50 \times 50 \times 50$ k-point grid, where $Ag - d$, $Bi - p$ and $I - p$ orbitals are used as basis to construct the Wannier functions. The effective masses are evaluated via a degenerate perturbation k.p approach with the direct evaluation of the velocity and momentum matrix elements, as implemented on the *mstar* code by O. Rubel *et al.*[6] These calculations include 1000 bands for the evaluation of the optical matrix. The radial distribution functions (RDF) are evaluated using the code Module for ab initio structure evolution (MAISE).[7]

2 Spectroscopic limited maximum efficiency

The most classical parameter employed to have a first glimpse on photovoltaic potential and capabilities of a material is the so called Schockley-Queisser limit (SQ).[8] The SQ is a measure of the maximum theoretical efficiency of a solar cell device using a simple single p-n junction under illumination of a standard solar/black-body spectrum. Due to its simplistic usage and dependency only on the fundamental band-gap of a material, the approach has been widely applied for the search of new photovoltaic absorbers. Yet, the SQ theory does not take into account dipole-forbidden transitions or the indirect band-gap character of some semiconductors. Moreover, the absorption coefficient of any material is taken into account as a step function of the form:

$$\alpha(E) = \begin{cases} 1\,; & E \geq E_g \\ 0\,; & E < E_g \end{cases}$$

where $\alpha(E)$ is the absorption coefficient and E_g is the band-gap. As so, a model which is capable of incorporating the true band-gap nature and absorption coefficient of materials is desirable.

The spectroscopic limited maximum efficiency (SLME) was proposed by L. Yu and A. Zunger as a mean to treat these problems and introduce ab-initio data directly into such models. As on the SQ limit, the power conversion efficiency of a solar cell device can be expressed as $\eta = \frac{P_m}{P_{in}}$, where P_m represents the maximum power that can be generated by the device assuming that the total solar power reaching it is P_{in}. The later can be obtained by integrating the solar irradiation over the energies, that is, $P_{in} = \int_0^\infty E I_{sun}(E) dE$. The maximum power can be obtained through the maximization of the $P(V)$ power function with respect the the voltage V:

$$P_m = max[J_{sc} - J_0(e^{eV/kT} - 1)]V_V.$$

Although here the expression are the same as in the SQ limit, the definitions of J_{sc} and J_0 are different. Here the absorptivity of the material is defined as $a(E) = 1 - e^{-2\alpha(E)L}$, where $\alpha(E)$ is the ab-initio evaluated absorption coefficient and L is the thin-film thickness.[9] The thickness dependence allows one to have a better understanding of photovoltaic properties of the materials. The short-circuit current can be determined as:

$$J_{sc} = e \int_0^\infty a(E) I_{sun}(E) dE, \tag{1}$$

where e is the electron charge.

Besides the thickness dependent absorptivity, the fraction of the radiative recombination current f_r is also taken into account (in SQ $f_r = 1$), to compute the reverse saturation current J_0. Thus, not all photons that reach the solar cell device will be absorbed, and the rate of photon absorption will depend intrinsically on the band-gap nature of the material, as follows:

$$J_0 = \frac{J_0^r}{f_r} = \frac{e\pi \int_0^\infty a(E) I_{bb}(E,T) dE}{e^{\Delta/kT}}.$$

The radiative recombination current J_0^r is evaluated through the absorptivity and the black-body spectrum $I_{bb}(E,T)$, and $\Delta = E_g - E_g^{da}$ represents the difference between the fundamental band-gap E_g and the true dipole-allowed direct band-gap E_g^{da}. The introduction of Δ allow us to differentiate materials by their optical type such as indirect or dipole-forbidden direct band-gap materials while f_r allows one to take into account the fraction of radiative recombinating e-h pairs.

The method was implemented in Fortran using the Fortran Standard Library (https://stdlib.fortran-lang.org) to perform the required integrals and function minimization. Furthermore, a third-order spline method was used to interpolate the ab-initio absorption coefficient over the experimental energy grid of the AM1.5G solar spectrum. The reference Air Mass 1.5G Spectra was obtained from the U.S. Department of Energy (DOE)/NREL/ALLIANCE data repository (www.nrel.gov/grid/solar-resource/spectra-am1.5.html), complying with the legal requirements for its usage.

3 Transformation matrices

Let **M** be the rotation transformation matrix that connects the basis vectors of the parent space-group **P** and the subgroup **S**, such as that **S** = **PM**. And let **m** be the translation matrix which transforms the origin **p** of the parent space-group into **s** of the subgroup, such as **s** = **pm**.

The pair of matrices **M** and **m** that connects the Fd$\bar{3}$m (227) to Imma (74) read:

$$\begin{bmatrix} 1/2 & 1/2 & 0 \\ -1/2 & 1/2 & 0 \\ 0 & 0 & 1 \end{bmatrix} \begin{bmatrix} 1/4 \\ 1/4 \\ 0 \end{bmatrix}.$$

The pair of matrices **M** and **m** that connects the R3m (166) to C2/m (12) read:

$$\begin{bmatrix} 1/3 & -3 & 0 \\ -1/3 & -3 & 0 \\ 2/3 & 0 & -1 \end{bmatrix} \begin{bmatrix} 0 \\ 0 \\ 0 \end{bmatrix}.$$

4 Tables

Table S1 | DFT-PBE band-gaps for different orderings between Ag and Bi on the $AgBiI_4$ $Fd\bar{3}m$ (227) conventional (C_i) and primitive (P_j) unit cell, where $i = 1, ..., 5$ and $j = 1, 2$.

Orderings	C_1	C_2	C_3	C_4	C_5	P_1	P_2
Band Gap (eV)	0.54	0.38	0.40	0.43	0.58	0.37	0.38

Table S2 | DFT-PBE and DFT-PBE0 band gaps for $AgBiI_4$ and Ag_3BiI_6.

Band-gaps (eV)	PBE	PBE0
$AgBiI_4$	0.53	1.67
Ag_3BiI_6	0.80	1.74

Table S3 | Electron and hole effective masses for $AgBiI_4$ and Ag_3BiI_6.

	holes			electrons		
	m_1	m_2	m_3	m_1	m_2	m_3
$AgBiI_4$	0.59	0.69	1.27	0.65	0.24	0.69
Ag_3BiI_6	0.57	0.59	0.54	0.65	0.61	0.44

Table S4 | Summary of the device properties obtained within the 300 nm SLME model and Shockley-Queisser limit. The experimental band-gap was used as input parameter for the later.

	SLME			SQ		
	PCE (%)	J_{sc} (mA/cm^2)	V_{oc} (V)	PCE	J_{sc} (mA/cm^2)	V_{oc} (V)
$AgBiI_4$	25.0	20.83	1.40	28.6	21.7	1.45
Ag_3BiI_6	21.6	17.99	1.45	26.5	18.8	1.54

5 Figures

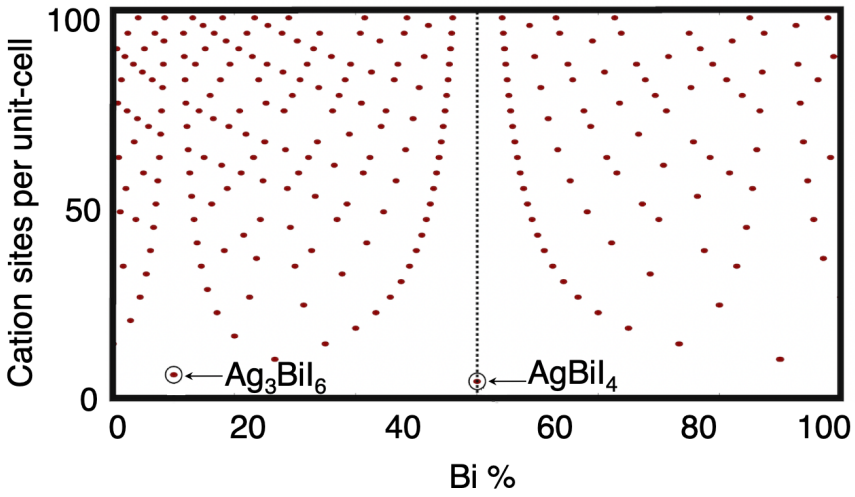

Figure S1 | Ag/Bi double salt material's phase space. Cation sites per unit cell as a function of the Bi to Ag ratio; every dot corresponds to a compound within the Ag/Bi halide double salts.

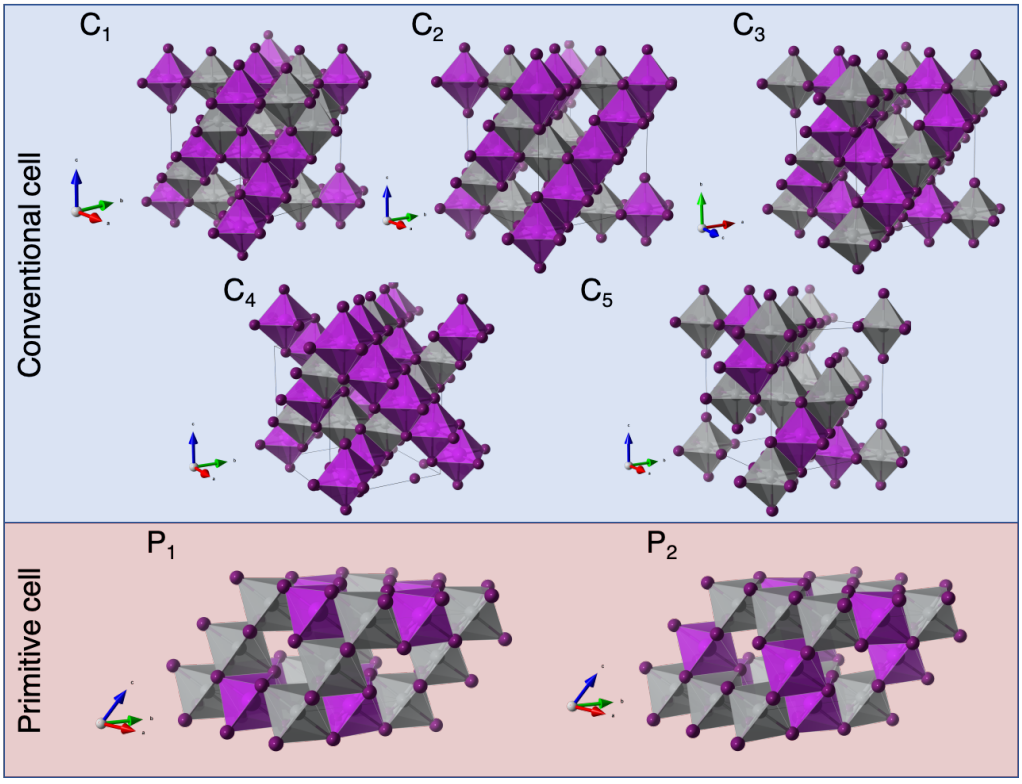

Figure S2 | Different atomic ordering for $AgBiI_4$ within the conventional cell (C_i) and primitive cell (P_j)

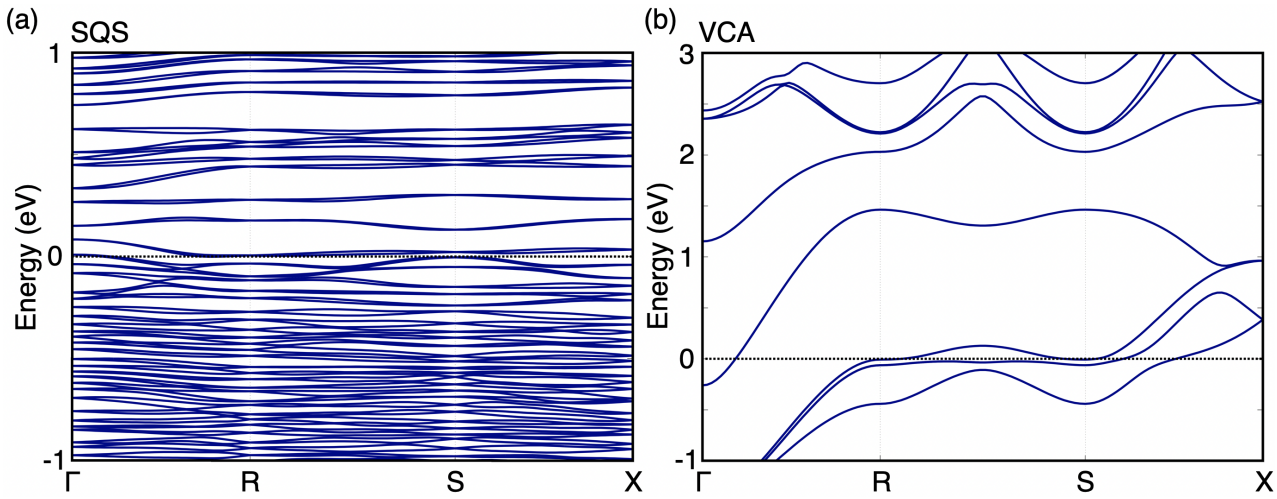

Figure S3 | (a) SQS and (b) VCA band structures for $AgBiI_4$ obtained with DFT-PBE calculations. (The Fermi energy is set at 0 eV.)

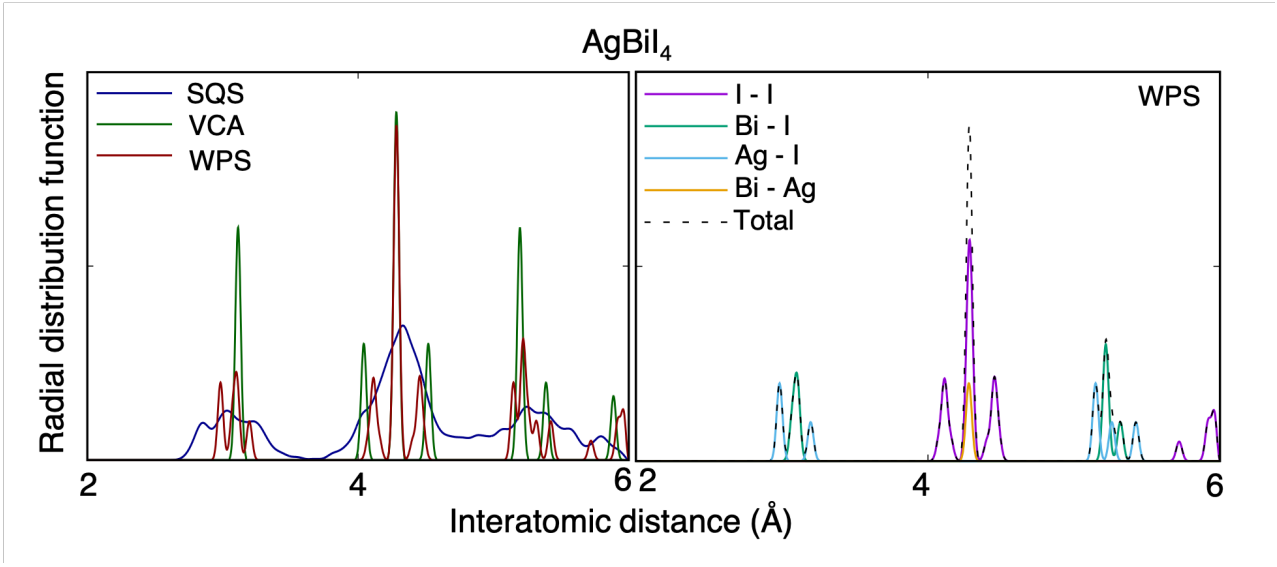

Figure S4 | Radial distribution functions calculated for the three modelling approaches: special quasi-random structures (SQS), virtual crystal approximation (VCA) and Wyckoff position splitting (WPS). Decomposition of of the radial distribution function for the case of the WPS to each pair of atomic species.

References

[1] P. Giannozzi, O. Andreussi, T. Brumme, O. Bunau, M. B. Nardelli, M. Calandra, R. Car, C. Cavazzoni, D. Ceresoli, M. Cococcioni, N. Colonna, I. Carnimeo, A. D. Corso, S. de Gironcoli, P. Delugas, R. A. DiStasio, A. Ferretti, A. Floris, G. Fratesi, G. Fugallo, R. Gebauer, U. Gerstmann, F. Giustino, T. Gorni, J. Jia, M. Kawamura, H.-Y. Ko, A. Kokalj, E. Küçükbenli, M. Lazzeri, M. Marsili, N. Marzari, F. Mauri, N. L. Nguyen, H.-V. Nguyen, A. O. de-la Roza, L. Paulatto, S. Poncé, D. Rocca, R. Sabatini, B. Santra, M. Schlipf, A. P. Seitsonen, A. Smogunov, I. Timrov, T. Thonhauser, P. Umari, N. Vast, X. Wu, S. Baroni, *J. Phys. Condens. Matter* **2017**, *29* 465901.

[2] P. Giannozzi, S. Baroni, N. Bonini, M. Calandra, R. Car, C. Cavazzoni, D. Ceresoli, G. L. Chiarotti, M. Cococcioni, I. Dabo, A. D. Corso, S. de Gironcoli, S. Fabris, G. Fratesi, R. Gebauer, U. Gerstmann, C. Gougoussis, A. Kokalj, M. Lazzeri, L. Martin-Samos, N. Marzari, F. Mauri, R. Mazzarello, S. Paolini, A. Pasquarello, L. Paulatto, C. Sbraccia, S. Scandolo, G. Sclauzero, A. P. Seitsonen, A. Smogunov, P. Umari, R. M. Wentzcovitch, *J. Phys. Condens. Matter.* **2009**, *21* 395502.

[3] M. van Setten, M. Giantomassi, E. Bousquet, M. Verstraete, D. Hamann, X. Gonze, G.-M. Rignanese, *Comput. Phys. Commun.* **2018**, *226* 39.

[4] D. Sangalli, A. Ferretti, H. Miranda, C. Attaccalite, I. Marri, E. Cannuccia, P. Melo, M. Marsili, F. Paleari, A. Marrazzo, G. Prandini, P. Bonfà, M. O. Atambo, F. Affinito, M. Palummo, A. Molina-Sánchez, C. Hogan, M. Grüning, D. Varsano, A. Marini, *J. Phys. Condens. Matter.* **2019**, *31* 325902.

[5] A. A. Mostofi, J. R. Yates, G. Pizzi, Y.-S. Lee, I. Souza, D. Vanderbilt, N. Marzari, *Comput. Phys. Commun.* **2014**, *185* 2309.

[6] O. Rubel, F. Tran, X. Rocquefelte, P. Blaha, *Comput. Phys. Commun.* **2021**, *261* 107648.

[7] S. Hajinazar, A. Thorn, E. D. Sandoval, S. Kharabadze, A. N. Kolmogorov, *Comput. Phys. Commun.* **2021**, *259* 107679.

[8] W. Shockley, H. J. Queisser, *J. Appl. Phys.* **1961**, *32* 510.

[9] T. Tiedje, E. Yablonovitch, G. Cody, B. Brooks, *IEEE Trans. Electron Devices* **1984**, *31* 711.